13

Low-Energy Photon Detection with PWO-II Scintillators and Avalanche Photodiodes in Application to High-Energy Gamma-Ray Calorimetry

Dmytro Melnychuk and Boguslaw Zwieglinski
The Andrzej Soltan Institute for Nuclear Studies, Hoza 69, PL-00681 Warsaw Poland

1. Introduction

APDs (Avalanche Photodiodes) referred to in this Chapter differ by their construction and characteristics from those commonly used in long-distance optical communication. Common to both applications is the usage of an internal gain mechanism that functions by applying an adequate reverse voltage. In the optical communication industry one is mainly interested in small diameter devices to be coupled to optical fibres in near infrared domain. In nuclear physics they are used to convert light pulses, induced by particles and photons in scintillating crystals, into electronic signals. These emit at shorter wavelengths, moreover, it is advantageous to cover up to several cm^2 of scintillator exit face with the sensing element to maximize the detector signal for low energies deposited in the scintillator. Therefore, progress in large area APDs in short-wavelength domain has been mainly driven by nuclear physics applications. A vast amount of research and development work invested by the joint CERN + Hamamatsu Photonics team resulted in a 5x5 mm^2 device (S8664-55), which paved the way to larger area APDs. A notable feature of S8664-55 is its outstanding radiation hardness, so that by its application, the CMS-ECAL expects 10 years of failureless operation in a hostile radiation environment of the CERN-LHC. Let numbers illustrate the volume of APD usage: the barrel part of CMS-ECAL has 122400 pieces and the ALICE-PHOS 35840 of them.
The meaning of the term *High-Energy Gamma-Ray* used in the title and meant in the rest of this chapter is related roughly to the maximum antiproton energy of 14 GeV from the HESR accumulator at the future FAIR facility in Darmstadt. The electromagnetic calorimeter (EMC) (Erni et al., 2008) of the PANDA detector, to be used in studies of hadron physics in antiproton-proton annihillations, will thus deal with photons in the energy range extending nearly from zero up to the maximum energy of the order of 10 GeV. *Low-Energy Photon* does not have its common meaning of a photon emitted from a radioactive source but rather is related to the practically achievable EMC low-energy detection threshold of several MeV. The results reported in Sect. 7 refer to a study intended to investigate detector resolution with 4 - 20 MeV photons, relevant for the latter energy range. Low-energy proton capture reactions are used to generate these gamma-rays.
A reader interested in medical application of APDs, for example in Positron Emission Tomography (PET), which uses photons emitted in annihilation of positrons from radioactive

sources, will find useful references in (Phelps, 2006). For additional data a review paper of (Moszynski et al., 2002) is recommended.

2. High-energy gamma-ray detection with inorganic scintillators

The choice of material of an individual EMC detection cell is related to the nature of high-energy photon interaction with matter. This initiates an electromagnetic cascade (shower) as e^+/e^- pair production and bremsstrahlung induced by them in the medium generate more electrons and photons with lower energy. Electron energies eventually fall below the critical energy, and then dissipate their energy by ionization and excitation, rather than by generation of more shower particles. In this way the cascade terminates. The spacial distribution of a shower is determined by radiation length, X_0, in longitudinal direction, and Molière radius, R_M, in transverse direction relative to the photon propagation direction. A summary of X_0, R_M and other important parameters typifying scintillators

Parameter		CeF_3	LSO/LYSO:Ce	BGO	PWO	PWO-II
ρ	g/cm^3	6.16	7.40	7.13	8.3	
X_0	cm	1.77	1.14	1.12	0.89	
R_M	cm	2.60	2.07	2.23	2.00	
τ_{decay}	ns	30	40	300	$30^s/10^f$	$30.4^s/6.5^f$
λ_{max}	nm	330	402	480	$425^s/420^f$	
n at λ_{max}		1.63	1.82	2.15	2.20	2.17
relative LY	%(LY NaI)	5	83	21	$0.083^s/0.29^f$ at RT 0.8 at -25°C	0.6 at RT 2.5 at -25°C
hygroscopic		no	no	no	no	
dLY/dT	%/°C	0.1	-0.2	-0.9	- 2.7 at RT	-3.0 at RT
dE/dx (MIP)	MeV/cm	6.2	9.6	9.0	10.1	

Table 1. Properties of a few scintillators used or planned to be used in high-energy gamma-ray calorimetry. f = fast component, s = slow component. The light yield of NaI(Tl), taken here as a reference, is 40000±2000 photons/MeV (Moszynski et al., 2002).

already used (BGO, PWO) or planned to be used (PWO-II, LSO/LYSO:Ce) in high-energy photon calorimetry is collected in Table 1. One may note an inverse correlation of X_0, R_M with, ρ, the material density. $PbWO_4$ (standard abbreviation PWO), posessing the highest density among those listed, thus offers the most compact calorimeter design, a valuable feature in view of the cost increasing as cube of the scintillator length. Economy considerations plus a short scintillation decay time, $\tau_{decay} = 6.5$ ns, motivated the PANDA Collaboration to choose PWO as the EMC material. The latter is important in order to assure short response time, necessary at high counting rates, expected to occur at small angles relative to antiproton beam direction. As the shape of an individual scintillator a truncated pyramid was decided with the front face of 20.2×20.2 mm and 200 mm (roughly $22 \cdot X_0$) length, which guarantees a tolerable energy loss due to longitudinal leakage of the shower in the forseen photon energy range. Further perfection of the PWO technology during the last decade resulted in the development of PWO-II (Novotny et al., 2005), (Borisevich et al., 2005) with doubled light yield at room temperature relative to that reported by CMS, e.g. in (Annenkov et al., 2002), and listed in Table 1. The improvement was reached by the producer - Bogoroditsk Plant of Technochemical Products (BTCP) in Russia by growing the crystals from melt with precise tuning of the stoichiometry and co-doping with Y and La with a total concentration

up to 40 ppm. To achieve further increase in light yield PANDA-EMC will be operated at a reduced temperature of T=-25°C extending electromagnetic calorimetry with sufficient energy resolution down to photon energies of a few MeV.

Lutetium oxyorthosylicate (Lu_2SiO_5:Ce or LSO) and lutetium-yttrium oxyorthosylicate ($Lu_{2(1-x)}Y_{2x}SiO_5$:Ce or LYSO) by their large light output, significantly larger than PWO, and fast decay time are the scintillators of the future, see e.g. (Ren-yuan Zhu et al., 2007). However, the present high cost associated with fabrication of scintillators with sufficient length was an obstacle to plan their usage in PANDA. The situation may improve with time, hence it is not excluded that the calorimeters of the planned SLHC and ILC will see application of LSO or LYSO.

Besides EMC the PANDA detector will contain other subsystems used for charged-particle identification and tracking goals. For the latter purpose the central part of the detector will work inside magnetic field, up to 2.0 T, of a superconducting solenoid. This precludes application of standard photomultiplier tubes as sensors for PWO-II readout. Led by the successful application of avalanche photodiodes (APDs) in PWO calorimetry by the CMS (Deiters et al., 2000) and ALICE (Aleksandrov et al., 2005) Collaborations at CERN, the PANDA Collaboration initiated a collaborative effort with the Hamamatsu Photonics K.K. (Japan) in order to develop an APD with a significantly larger sensitive area than 5×5 mm^2 posessed by S8664-55 used in those detectors. This was required by significantly lower energies of photons, as indicated above, to be encountered with PANDA in comparison with multi-GeV deposits in the search for Higgs boson at the CERN-LHC. An APD S8664-1010 with the sensitive area 10×10 mm^2 was developed to meet the needs of PANDA Collaboration for the initial R&D stage of the EMC. Ultimately, an application of two 20×10 mm^2 Hamamatsu APDs is forseen completely covering the exit face of a scintillator.

3. Principle of operation of an APD

The principle of operation of an Si APD, used in conjunction with PWO, or any other scintillator emitting short wavelength light, which is strongly absorbed in Si, is illustrated with the aid of Fig. 1. The basic elements of an APD are contained between the cathode and anode contacts reversed biased with the positive potential on the cathode so that the wafer is fully depleted. The electic field, reaching values as high as $2.5 \cdot 10^5$ V/cm at the P-N junction, as a function of depth is indicated schematically. The surface, through which the detected light enters, is protected with an antireflective coating, Si_3N_4 or SiO_2, which improves the quantum efficiency by reducing reflection losses from the surface of the Si wafer. The P-type material in front of the amplification region, which forms the P-N junction (*buried junction*) is made less than 7 μm thick to reduce sensitivity to the *nuclear counter-effect*. For e-h pairs generated within the first few microns of the depletion layer, the electron is collected and undergoes full multiplication, whereas for a pair generated within the wide drift region behind the multiplying region only the hole enters the multiplying region, where it undergoes a much reduced gain. This additional layer of N-type material is introduced to decrease the APD capacitance and to improve stability with respect to changes in bias voltage. A notable feature is the groove cut around the p - n structure and slightly into the drift space (Deiters et al., 2000) (not shown in Fig. 1) to limit the surface currents.

The *nuclear counter-effect* refers to the situation when the charged component (e^+/e^-) of an electromagnetic shower leaks out through the rear face of the scintillator and causes ionization in the attached light sensor. This is an undesired effect, since it superimposes the signal produced by scintillation light causing a decrease in its resolution. Comparing an APD with

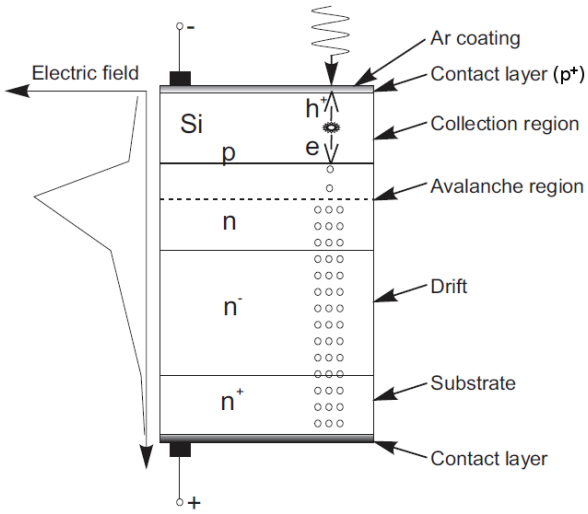

Fig. 1. The concept of an Si APD intended for short-wavelength light detection is demonstrated with a section of the Si wafer. The electric field distribution, $E(x)$, is plotted schematically to the left of the structure. Broken line marks the position of a P-N junction. Note that relative thicknesses of the different regions are not shown in scale. Ar coating is an abbreviation for Anti-reflective coating.

a PIN diode of the same thickness, one concludes that the *nuclear counter-effect* is very much reduced in the former because of a narrow width of the collection region (see above).

4. Energy resolution of an APD in scintillation light detection

The performance of an APD depends on the number of primary electron-hole (e-h) pairs produced by scintillation light, N_{eh}, APD excess noise factor, F, and dark noise level of the device-preamplifier system. The quantum efficiency, $\epsilon_Q(\lambda)$, of the APD and spectral distribution of the light emitted by a scintillator, $N_{phot}(\lambda)$, define the number of (e-h) pairs. The excess noise is due to the statistical nature of the multiplication process, which causes additional fluctuation of the measured signal. The excess noise factor depends on the ratio, $k = \beta(E)/\alpha(E)$, of ionization coefficients for electrons, $\alpha(E)$, and holes, $\beta(E)$, both functions of the electric field, E. F is a function of the internal structure of the diode, profile of the electric field and the device operating gain. The statistical variance of the APD signal, σ_N^2, is expressed as:

$$\sigma_N^2 = M^2\sigma_n^2 + N_{eh}\sigma_A^2, \tag{1}$$

where, σ_N^2, is the variance of the output signal, expressed in the number of electrons, M, is the APD gain, σ_n^2 is the variance of the number of primary electrons and σ_A^2 is the variance of single electron gain. Dividing both sides of Eq. 1 with M^2 and taking into account the definition of F:

$$F = 1 + \sigma_A^2/M^2, \tag{2}$$

we get the statistical variance of the signal from an APD, σ_{st}^2:

$$\sigma_{st}^2 = \sigma_n^2 + N_{eh}(F-1). \tag{3}$$

The first term in Eq. 3 corresponds to the statistical error of the detected signal, while the second one to the contribution of the avalanche gain of an APD. Taking into account that σ_n^2 is governed by Poisson statistics:

$$\sigma_n^2 = N_{eh}, \tag{4}$$

we find that the variance of APD signal is given by:

$$\sigma_{st}^2 = N_{eh}F. \tag{5}$$

Assuming that the detected peak is Gaussian and taking into account the relation between its variance and full width at half maximum (FWHM), we may write that the FWHM resolution is:

$$(\Delta E)^2 = (2.36)^2(N_{eh}F + \delta_{noise}^2), \tag{6}$$

where the dark noise contribution δ_{noise}, expressed in rms electrons has been explicitely included. One may rewrite Eq. 6 in energy units by taking into account that ε=3.6 eV is required for one e-h pair creation in Si:

$$(\Delta E)^2 = (2.36)^2(FE\varepsilon + \Delta_{noise}^2), \tag{7}$$

where Δ_{noise} is the dark noise contribution of the diode-preamplifier system (FWHM in energy units). The relative energy resolution (in %) is:

$$\Delta E/E = 2.36(F/N_{eh} + \delta_{noise}^2/N_{eh}^2)^{1/2}. \tag{8}$$

One may conclude from Eq. 8 that the relative energy resolution of the light signal is a decreasing function of both the number of primary e-h pairs and the signal-to-noise ratio. The high light output of a scintillator and high quantum efficiency of the employed APD are of primary importance to reduce $\Delta E/E$.

4.1 Dark noise contribution to energy resolution

The sources of dark noise in Eq. 6 are parallel and series noise of an APD. The parallel noise originates from the surface and bulk dark currents of the device. The series noise is the effect of shot noise of a preamplifier; it is proportional to the sum of APD capacitance and input capacitance of preamplifier. Following Ref. (Lorenz et al., 1994) we may write δ_{noise}^2 in Eq. 6 as:

$$\delta_{noise}^2 = 2q\left(\frac{I_{ds}}{M^2} + I_{db}\cdot F\right)\tau + 4kTR_s\frac{C_{tot}^2}{M^2}\frac{1}{\tau}, \tag{9}$$

where q is the electron charge, I_{ds} the surface leakage current, I_{db} the bulk current, τ the shaping time constant of the amplifier (assumed $\tau = \tau_{diff} = \tau_{int}$), k the Stephan-Boltzmann constant, T the absolute temperature, R_s the preamplifier series noise resistance, C_{tot} the parallel capacitance (APD plus preamplifier). We will show in Sect. 5 that APD capacitance decreases rapidly with the reverse bias voltage.

Fig. 2 illustrates the dependence of the noise contribution vs. gain for different shaping time constants of the amplifier. The measurements were performed in Ref. (Moszynski et al., 1997). The lowest noise contribution is observed close to the maximum attained gain of 160 and the shortest shaping time constant of 50 ns. Eq. 9 reflects the measured trends. The initial decrease of noise with APD gain is related to a simultaneous action of several factors: the attenuation of an unamplified noise component, related to I_{ds} in Eq. 9, decreasing capacitance of the APD with increasing bias voltage (see Fig. 3D) and the preamplifier noise. The curves have slightly increasing tendency at high gain, passed the minimum, because of dark current excess noise and fluctuations in avalanche gain, both of which increase with the excess noise factor,F.

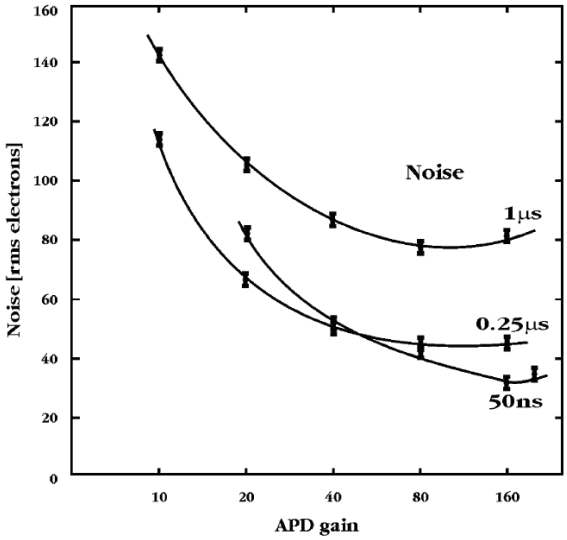

Fig. 2. Noise (in rms electrons) as a function of the gain for different shaping time constants measured in (Moszynski et al., 1997) [*reproduced from (Moszynski et al., 2002) with permission of Elsevier Ltd*].

5. Main characteristics of Hamamatsu silicon APDs

The quantum efficiency of Hamamatsu APDs S8664-55/S8664-1010 as a function of light wavelength is presented in Fig. 3A. One may see that at the wavelength of 420 nm, corresponding to the maximum of PWO blue emission (see Table 1), the efficiency is above 70% and shows a broad plateau thereafter with an efficiency of about 85%. This should be compared with about 18% of a typical photomultiplier with a bialkali photocathode in the same spectral range. One may conclude that these APDs are very well matched for detection of light from PWO. Light absorbed behind the P-N junction in Fig. 1 produces electrons and holes, but only holes go to the avalanche region and multiply, while electrons drift towards the back contact and are collected without multiplication. The multiplication factor for holes is much smaller than that for electrons, as a result the gain for light with long wavelengths is smaller than for short ones, which is reflected also as a drop with wavelength in Fig. 3A in the quantum efficiency.

Fig. 3B presents plots of gain vs. reverse voltage at the different working temperatures. With increasing voltage these curves approach the breakdown voltage, which is characterized by an uncontrollable growth of the dark current (see Fig. 3C). On the other hand, the asymptotic value of gain at low voltages is unity (not reached in Fig. 3B), at which carriers created in the collection region are transferred though the p-n junction without multiplication. A typical operating gain used with the indicated APDs is M=50 at room temperature, +20 °C. One may note that decreasing the temperature down to -20 °C, which is close to the forseen operating temperature of PANDA at -25 °C, will bring an increase of about a factor of 3 - 3.5 in gain. This increase in gain is ascribed to decreasing excitation of lattice phonons, which permits carriers to acquire higher energies used in avalanche multiplication. One may conclude that both these operating parameters, voltage and temperature, should be carefully stabilized for

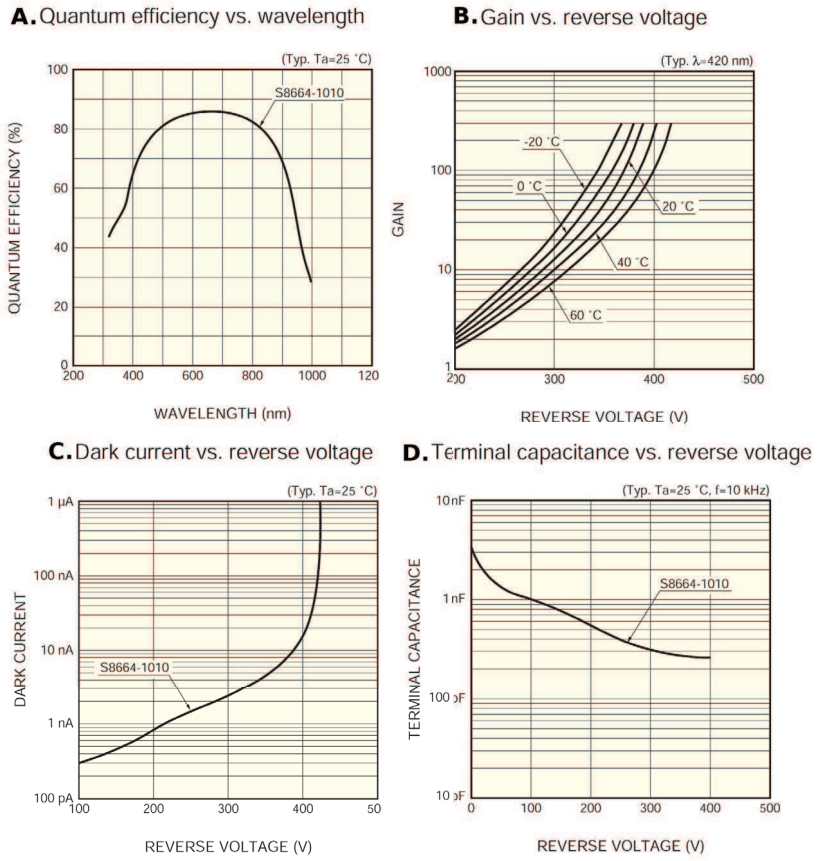

Fig. 3. Selected characteristics of an APD S8664-1010 of Hamamatsu Photonics K.K. [*by courtesy of Hamamatsu Photonics K.K.*].

a stable operation. The bias at room temperature cannot be chosen too high, because cooling that follows, may end-up in break-down. M=50 is a safe initial choice, as proved in practice, with the corresponding voltage and reverse current values at room temperature provided for each APD by the producer. A further fine tuning of gain is accomplished by distributing a reference light signal through a system of optical fibers in contact with an exit face of each individual scintillator.

Comparing Hamamatsu Si-APDs with other producers, one notes several additional features making the Japanese products more convenient in large-scale application, as in the PANDA-EMC. The silicon wafer of S8664-1010 is installed on a thin ceramic plate, only slightly exceeding in size the sensitive area 10×10 mm^2. Moreover, the surface through which light enters is covered with a transparent plastics. This prevents from damaging the APD upon exerting stress when a contact with the scintillator is done using an optical grease. Also, much lower bias voltage at the same gain deserves stressing as a factor in favor of Hamamatsu in large-scale applications.

6. Measurements of $\Delta E/E$ using high-energy tagged photon beams and detector matrices

A comprehensive information on the performance of a PWO+APD combination is obtained from an experiment in which the PWO scintillator is irradiated along its axis with a narrow beam of photons and the scintillation light converted into an electronic signal with the aid of an APD. It has been stressed in Sect. 2 that high-energy photons create an electron-positron shower, which propagates both along and perpendicular to the scintillator axis. The lateral dimensions of scintillators of about 20×20 mm^2 are determined by the required angular resolution [*granularity*] in the forseen experiments (see (Erni et al., 2009)). With the Molière radius (see Table 1) of 2.0 cm for PWO, one needs a matrix of at least nine closely packed scintillators in order to intercept with the scintillating material and convert into light the shower originating from the central one. An experiment using high-energy tagged photons is illustrated in Fig. 4. Photons are products of bremsstrahlung of a high energy electron beam from the MAMI-B microtron facility at Mainz in a thin carbon foil. There is a unique relation between the energy of a photon and the momentum of an electron that it radiated, so that the highest energy photons are accompanied with low-momentum electrons and *vice-versa*. The post-radiation electron is bent in the magnetic field of a magnetic spectrometer and detected with a position-sensitive detector along its focal plane. This illustrates the method of *photon-tagging* with the aid of coincident electron detection in a certain range of positions

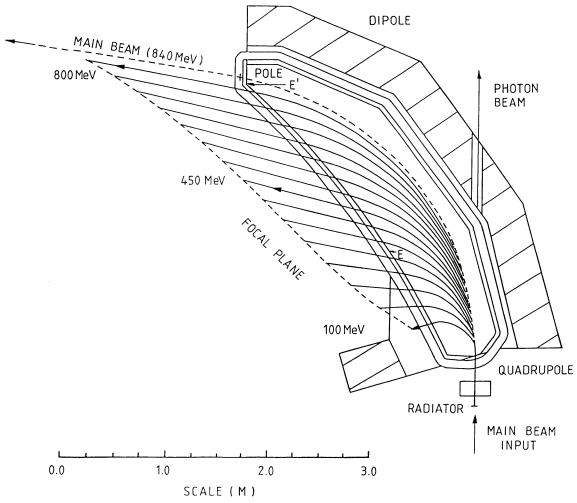

Fig. 4. Section of the magnetic spectrometer of the MAMI-B tagging facility along its central plane. The iron flux return yoke is shown hatched. The dotted line is the trajectory of electrons with the incident momentum. The solid lines are trajectories of electrons that suffered bremsstrahlung with emission of photons with progressively increasing energy. The matrix of nine PWO-II scintillators is located behind an iron collimator (not shown) with its central scintillator axis along the photon beam [*reproduced from (Anthony et al., 1991) with permission of Elsevier Ltd*].

in the focal plane (Anthony et al., 1991; Hall et al., 1996). In the experiment that we refer to (Novotny et al., 2008) sixteen photon energies in the range 40.9 - 674.5 MeV were selected, and

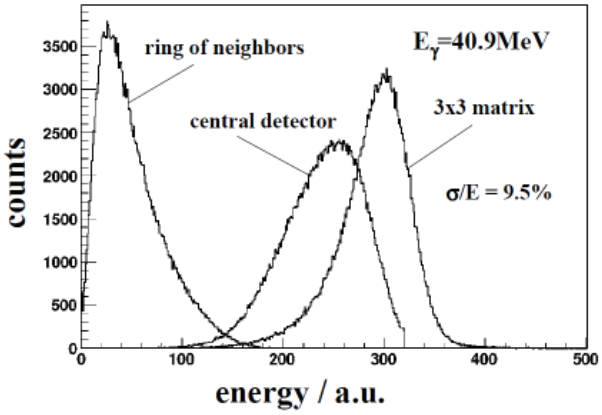

Fig. 5. Amplitude spectra illustrating the response of the central scintillator and the entire 3x3 PWO-II matrix, taken eventwise, to photons with E_γ= 40.9 MeV selected with the MAMI tagger. The matrix was kept at 0°C [*reproduced from (Novotny et al., 2008a)*].

the primary electron beam energy was 840 MeV. Typical energy width per tagging channel varied between 2.3 MeV at 50 MeV to 1.5 MeV at 500 MeV photon energy, respectively. The matrix of 3x3 PWO-II scintillators was installed in a thermally isolated container, in which it was cooled down to 0°C. The container could be moved remotely in the plane perpendicular to the photon beam, so that each of the nine scintillators could be inserted into the beam and its amplitude spectra calibrated in energy at the sixteen points. After the calibration runs, the central scintillator was inserted and the spectra in all of them simultaneously measured. By summing eventwise the energy deposits, the energy response to a photon shower for the entire matrix was determined. Fig. 5 compares the spectrum in the central scintillator with the result of summing individual scintillator responses eventwise for the incident photon energy E_γ= 40.9 MeV. The summed spectrum is almost Gaussian, with only a slight indication of the tailing seen. The reduced Gaussian widths, σ/E, of the summed peaks, are plotted in Fig. 6 as a function of the photon energy. The solid line is a fit to the measured points with a formula:

$$\frac{\sigma}{E} = \frac{1.86\%}{\sqrt{E[GeV]}} + 0.65\%, \tag{10}$$

where the energy is expressed in GeV. One recognizes here Eq. 8 with the first statistical, and the second constant term. A comparison with the GEANT4 simulations (lower curve in Fig. 6), which considers just the pure energy deposition into the scintillator material, demonstrates the contribution due to photon statistics and the effect of experimental thresholds. The resolution approaches asymptotically the simulation reflecting the decreasing relative importance of the latter two factors. The value obtained by extrapolating Eq. 10 to 1.0 GeV is 2.5% - best resolution ever measured at this energy for PWO with APD readout. One should stress that energies lower than 40.9 MeV could not be reached with the MAMI photon tagger, having the maximum photon energy set at 674.5 MeV, because of limitations imposed by the focal plane detector.

7. Measurements of $\Delta E/E$ using low-energy photons produced in proton capture reactions

Identification of π^0 and η mesons by detecting both γ-rays from their decay is a prerequisite for suppressing undesired background in studies of photon transitions between the states of charmonium in the physics program of PANDA (Erni et al., 2009). The detection threshold of the PANDA - EMC should be as low as possible to achieve this goal. Thus the question arises, whether the relative resolution, $\sigma(E)/E$, will or will not follow Eq. 10 at energies lower than 40.9 MeV, where it is expected to deteriorate rapidly because of $\sqrt{E}$ term in the denominator. The authors of Ref. (Melnychuk et al., 2009) decided to answer this question using gamma-rays produced in proton-induced reactions with light nuclei. The reactions ^{11}B(p,γ)^{12}C and T(p,γ)^{4}He are of primary concern, because they proceed to well-separated, narrow states in the final nuclei, so that the photon energy spread is determined by the target thickness and beam energy spread. These two factors gave negligible contribution to σ/E in the reported experiment. In order to make a direct comparison with the results of (Novotny et al., 2008) and Eq. 10, we used a PWO-II scintillator of the same size $20\times20\times200$ mm, as used in the scintillator matrix of Sect. 6, the same type of reflector, an APD S8664-1010 of Hamamatsu Photonics and the same preamp type LNP as used in that work. What differed our experiments was the working temperature. We aimed at -25°C, forseen as the working temperature for PANDA, however reached only -21.6 °C, because of insufficient cooling power of our JULABO F32-ME refrigerated circulator and thermal losses from the cooled volume to the ambient.

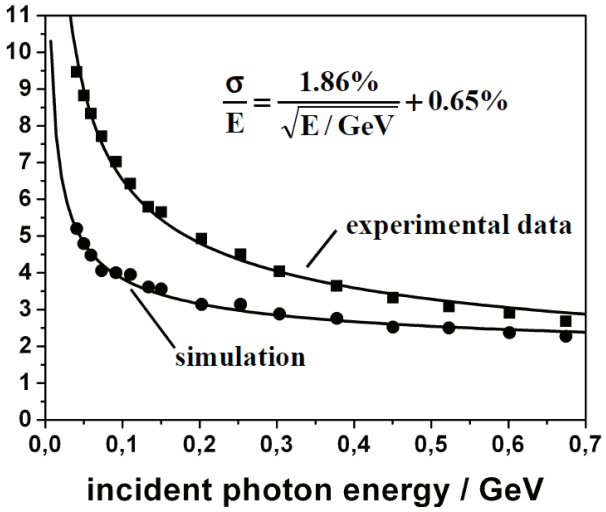

Fig. 6. Experimental reduced energy resolutions, σ/E, (upper set of points) and the results of GEANT4 simulations (lower set) for the 3x3 PWO-II matrix in the energy range 40.9 - 674.5 MeV. The simulation incorporates only the pure energy deposit. Solid lines are the results of fits, with the upper line given by the indicated formula [*reproduced from (Novotny et al., 2008a)*].

An isolation from the ambient is provided in our system by vacuum common with the Van-de-Graaff accelerator, which was 3 - 7×10^{-6} mbar in the performed measurements. Our

experimental system is intended for PWO response measurements in the energy range 4.4 - 20 MeV, which is accessible with the aid of the above mentioned reactions. In this energy range pair production is the main interaction process of photons with heavy elements as occuring in $PbWO_4$. Consequently, we used a cylinder of the plastic scintillator EJ-200, cut along the vertical axis, which covered the PWO-II over the length of 13.4 cm. Both halves were readout independently via light-guides with the 3 inch diam. photomultipliers XP4312.
A detailed presentation of the experimental system is contained in Ref. (Melnychuk et al., 2009). The PWO-II received photons along its axis through a lead collimator from the beam spot on a ^{11}B target. The events in which an electron-positron pair was generated within its volume, and both 0.511 MeV positron annihilation quanta absorbed therein, could be separated with the aid of the two plastics from the events in which one or both of the annihilation quanta escaped from the PWO-II and ended up to be detected in the plastics. The spectra from these three channels were registered with a 14-bit 100 MHz sampling ADC N1728B of CAEN. Fig. 7 is the full-energy spectrum in PWO sorted-out using the above mentioned criterion. The solid line is a sum of the three Gaussians with indicated energies and reduced resolutions, σ/E, fitted to the spectrum. The two highest energy peaks correspond to gamma-ray transitions from the capturing state in ^{12}C to its ground and first excited states, respectively. An intense peak with E_γ=6.13 MeV originates from the 6.13 MeV state in ^{16}O, excited in $^{19}F(p,\alpha)^{16}O$ with a fluorine contamination of the ^{11}B target, because of its strong affinity to ^{19}F. A small contribution of the 6.92 and 7.12 MeV lines in ^{16}O is also taken into

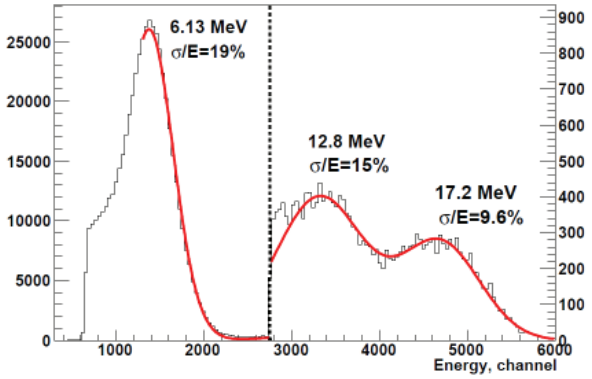

Fig. 7. Full-energy spectrum of γ-rays excited with the 1390 keV proton beam in a thin ^{11}B target, detected with the PWO-II scintillator cooled down to -21.6°C. The solid line is a fit with the three Gaussians. The relative dispersions, resulting from the fit, σ/E, are indicated [*reproduced from (Melnychuk et al., 2009) with permission of Elsevier Ltd*].

account. These assignments of the produced gamma-rays to proton induced reactions were obtained with a large NaI(Tl) detector offering a much better resolution than PWO with the same boron target. In order to compare our dispersions with the smooth trend established in Eq. 10, one needs to take into account the increase of light yield upon lowering the working temperature from 0°C in (Novotny et al., 2008) to -21.6 °C in (Melnychuk et al., 2009).
Taking into account the dependence of PWO-II light yield on the temperature, quoted in Ref. (Erni et al., 2008) one comes to a formula which should approximately govern σ/E, if both

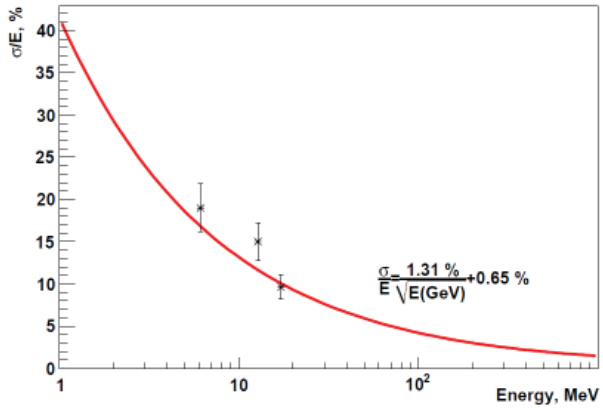

Fig. 8. Comparison of the relative dispersions, σ/E, measured in Ref. (Melnychuk et al., 2009) (points with error bars) with the smooth trend established in Ref. (Novotny et al., 2008) in the 40.9 - 674.5 MeV energy range at MAMI. The curve is corrected for the difference in working temperatures between these two experiments [*reproduced from (Melnychuk et al., 2009) with permission of Elsevier Ltd*].

experiments used -21.6°C:

$$\frac{\sigma}{E} = \frac{1.31\%}{\sqrt{E[GeV]}} + 0.65\%. \tag{11}$$

We have tacitely assumed in Eq. 11 that contributions to resolution beyond photon statistics in both experiments were equal. Eq. 11 is plotted with the solid line in Fig. 8. One may conclude from this figure that a smooth trend established in Ref. (Novotny et al., 2008) in the photon energy range 40.9 - 674.5 MeV gives a valid extrapolation of resolution for cooled PWO-II scintillators with APD readout to energies as low as 6 MeV. It should be stressed that with a tritium target and the T(p,γ)^{4}He reaction, which yields monoenergetic gammas with about 20 MeV energy at $E_p \approx 1$ MeV, a much simpler pattern than in Fig. 7 is expected. We plan to perform such an experiment in order to get a clean access to the line-shape to learn on its possible deviation from a pure Gaussian as implied in Fig. 5.

8. Summary

This Chapter is intended to give the interested reader an insight into application of APDs as sensors for the readout of scintillation light in multielement electromagnetic calorimeters. This application promotes high-energy and medium-energy nuclear physics to major users of large-area APDs in the blue domain of light spectrum, consequently nominates them to the title of driving force of large-area APD development. Sect. 1 introduces the main actors on the scene: CMS and ALICE Collaborations at the CERN-LHC at high-energies and the PANDA Collaboration at FAIR-Darmstadt in the medium-energy domain. The CMS-ECAL was the pioneer by its development together with Hamamatsu Photonics K.K. of an APD S8664-55, which fitted well the large light signals from over hundred-GeV photon detection in PWO. The PANDA Collaboration considered other options for a scintillator besides PWO, however, its fast scintillation decay time and good radiation hardness were the major factors to stay also with this scintillator choice. A significant R&D effort together with the Bogoroditsk

Plant of Technochemical Products (BTCP), the scintillator producer, has been invested into perfectioning the properties of PWO, which resulted in an improved version PWO-II, with doubled light output in comparison with the average used in the CMS-ECAL (Sect. 2). To achieve further increase in light yield it was decided to operate PANDA-EMC at a reduced temperature of -25°C.
A parallel research program conducted together with Hamamatsu Photonics K.K. resulted in an APD S8664-1010, having the sensitive area increased fourfold and posessing a superior radiation hardness of its predecessor. Sect. 3 is intended for a qualitative presentation of the essential features of S8664-1010 and explaining how its narrow *collection region* helps to minimize an adverse *nuclear counter effect*. Sect. 4 summarizes the factors determining energy resolution, which is manifested as a full-width at half maximum, ΔE, of an output signal of the sensor under excitation of the scintillator with monoenergetic photons. We use also an equivalent σ parameter of a Gaussian fitted to the line shape to characterize energy resolution. Sect. 4.1 extends the discussion to the dark-noise contribution to energy resolution and illustrates how this component is influenced by APD gain and shaping time-constant of the amplifier. Sect. 5 presents several characteristics of an APD S8664-1010 and relates them to the discussion in Sect. 4. Sections 6 and 7 are devoted to a detailed presentation of the methods used to measure the relative resolution, σ/E an important property of the scintillator plus APD combination, in a wide range of photon energies, i.e. light signals. The electron-photon avalanche at high photon energies requires application of the detector matrices (Sect. 6), whereas at low energies, where the first stage of a shower, the pair formation dominates, a simpler system might prove sufficient (Sect. 7). It is demonstrated that a smooth functional dependence of σ/E on the photon energy, E, established in (Novotny et al., 2008) (Sect. 6), when corrected for the difference in applied temperatures, accounts well also for the rapid increase of σ/E in the low-energy domain.

9. Acknowledgments

We gratefully acknowledge the effort of the staff and technical personnel of the SINS and JLUG Institutes in performing the measurements reported in this Chapter. The authors are grateful to Professor Rainer W. Novotny for the critical reading of the manuscript and constructive remarks, which greatly improved its quality. This work was supported in part by the European Community Framework Programme FP6 under Contracts #RII3-CT-2003-506078; Hadron Physics and #515873; DIRACsecondary-Beams (PANDA4). This work received also support on behalf of the Polish Ministry for Science and Education and the International Post-Graduate Studies of the Polish Academy of Sciences.

10. References

Aleksandrov, D.V. et al. (2005) *Nuclear Instr. and Meth. in Phys. Res. A*, Vol. 550, No. 1-2, September 2005, 169 - 184.

Annenkov, A.A. et al. (2002) *Nuclear Instr. and Meth. in Phys. Res. A*, Vol. 490, No. 1-2, Sept. 1 2002, 30 - 50.

Anthony, I. et al. (1991) *Nuclear Instr. and Meth. in Phys. Res. A*, Vol. 301, No. 2, March 1 1991, 230 - 240.

Borisevich, A. et al. (2005) *Nuclear Instr. and Meth. in Phys. Res. A*, Vol. 537, No. 1-2, Jan. 21 2005, 101 - 104.

J. Chen, L. Zhang and Ren-yuan Zhu, (2007) *Nuclear Instr. and Meth. in Phys. Res. A*, Vol. 572, No 1, March 1, 2007, 218 - 224.

Deiters, K. et al. (2000) *Nuclear Instr. and Meth. in Phys. Res. A*, Vol. 442, No. 1-3, March 2000, 193 - 197.

Erni, W. et al. (2008). *Technical Design Report for PANDA Electromagnetic Calorimeter (EMC)*, Heinsius F.-H., Kopf B., Lewandowski B., Löhner H., Novotny R., Peters K., Rosier Ph., Schmitt L., Vasiliev A., (Eds.), October 2008, 1 - 199, arXiv:0810.1216v1

Erni, W. et al. (2009). *Physics Performance Report for: P̄ANDA Strong Interaction Studies with Antiprotons*, Bettoni D., Bussa M.P., Düren M., Feliciello A., Gillitzer A., Iazzi F., Johansson T., Kopf B., Lehrach A., Lutz M.F.M., Mass F., Maggiora M., Negrini M., Peters K., Pochodzalla J., Schmitt L., Scholten O., Stancari G., Timmermans R., (Eds.), March 2009, 1 - 204, arXiv:0903.3905v1

Hall, S.J. et al. (1996) *Nuclear Instr. and Meth. in Phys. Res. A*, Vol. 368, No. 3, Jan. 11, 1996, 698 - 708.

Lorenz, E. et al. (1994) *Nuclear Instr. and Meth. in Phys. Res. A*, Vol. 344, No 1, April 21, 1994, 64 - 72.

Melnychuk, D. et al. (2009) *Nuclear Instr. and Meth. in Phys. Res. A*, Vol. 607, No. 3, Aug. 21, 2009, 600 - 606.

Moszynski, M. et al. (1997) *IEEE Trans. Nucl. Sci.*, Vol. NS-44, No 3, June 1997, 436 - 442.

Moszynski, M. et al. (2002) *Nuclear Instr. and Meth. in Phys. Res. A*, Vol. 485, No 3, June 11, 2002, 504 - 521.

Novotny, R.W., Döring W.M., Hjelm F., Melnychuk D., Makonyi K., Reiter A., Salz Ch., Steinacher M., Thiel M., Zwieglinski B. (2005) *IEEE Nucl. Sci. Symp. Conf. Record*, Oct. 23 - 29, 2005, 244 - 248, ISSN 1082 - 3654.

Novotny, R.W. et al. (2008) *IEEE Trans. Nucl. Sci.*, Vol. NS-55, No 3, June 2008, 1295 - 1298.

Novotny, R.W. et al. (2008a) *GSI Scientific Report 2007*, GSI Report 2008 - 1, (2008), 29.

Phelps, M.E. (2006). *PET - Physics, Instrumentation and Scanners*, Springer, ISBN-10: 0-387-32302-3, Berlin, Heidelberg, New York.

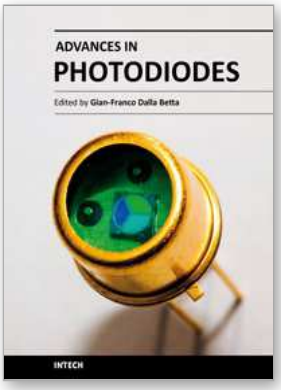

Advances in Photodiodes

Edited by Prof. Gian Franco Dalla Betta

ISBN 978-953-307-163-3
Hard cover, 466 pages
Publisher InTech
Published online 22, March, 2011
Published in print edition March, 2011

Photodiodes, the simplest but most versatile optoelectronic devices, are currently used in a variety of applications, including vision systems, optical interconnects, optical storage systems, photometry, particle physics, medical imaging, etc. Advances in Photodiodes addresses the state-of-the-art, latest developments and new trends in the field, covering theoretical aspects, design and simulation issues, processing techniques, experimental results, and applications. Written by internationally renowned experts, with contributions from universities, research institutes and industries, the book is a valuable reference tool for students, scientists, engineers, and researchers.

How to reference

In order to correctly reference this scholarly work, feel free to copy and paste the following:

Dmytro Melnychuk and Boguslaw Zwieglinski (2011). Low-Energy Photon Detection with PWO-II Scintillators and Avalanche Photodiodes in Application to High-Energy Gamma-Ray Calorimetry, Advances in Photodiodes, Prof. Gian Franco Dalla Betta (Ed.), ISBN: 978-953-307-163-3, InTech, Available from: http://www.intechopen.com/books/advances-in-photodiodes/low-energy-photon-detection-with-pwo-ii-scintillators-and-avalanche-photodiodes-in-application-to-hi

INTECH
open science | open minds

InTech Europe
University Campus STeP Ri
Slavka Krautzeka 83/A
51000 Rijeka, Croatia
Phone: +385 (51) 770 447
Fax: +385 (51) 686 166
www.intechopen.com

InTech China
Unit 405, Office Block, Hotel Equatorial Shanghai
No.65, Yan An Road (West), Shanghai, 200040, China
中国上海市延安西路65号上海国际贵都大饭店办公楼405单元
Phone: +86-21-62489820
Fax: +86-21-62489821